Microfluid Nanofluid (2014) 16:587–595
DOI 10.1007/s10404-013-1251-4

RESEARCH PAPER

A study on boundary force model used in multiscale simulations with non-periodic boundary condition

W. J. Zhou · H. B. Luan · Y. L. He · J. Sun · W. Q. Tao

Received: 17 April 2013 / Accepted: 13 August 2013 / Published online: 28 September 2013

Abstract This paper presents an investigation of the non-periodic boundary condition (NPBC) which is often used in multiscale atomistic–continuum simulations. The relationship between the boundary force exerted by the imaginary atoms outside the atomistic domain and the fluid state parameters including density and temperature at the boundary is studied. A fitting formula of the boundary force as a function of the fluid state has been proposed based on the relationship. The accuracy of the fitting formula is verified by the equilibrium molecular dynamics (MD) simulations. Poiseuille flow with viscous dissipation and unsteady heat transfer between two walls is then simulated using the proposed fitting formula. The elimination of density oscillation near the boundary of atomistic region and good agreement of velocity and temperature evolutions with time from pure MD and the multiscale simulations adopting NPBC further confirm the correctness of our fitting formula.

Keywords Multiscale simulation · Finite volume method · Molecular dynamics simulation · Non-periodic boundary condition · Boundary force

W. J. Zhou · Y. L. He · W. Q. Tao (✉)
Key Laboratory of Thermo-Fluid Science and Engineering of MOE, School of Energy and Power Engineering, Xi'an Jiaotong University, 710049 Shaanxi, Xi'an, People's Republic of China
e-mail: wqtao@mail.xjtu.edu.cn

H. B. Luan
Shanghai Marine Diesel Engine Research Institute, 201108 Shanghai, People's Republic of China

J. Sun
Institute of Engineering Thermophysics, Chinese Academy of Sciences, 100190 Beijing, People's Republic of China

1 Introduction

With the development of nanotechnology, more and more attention has been paid to the micro- and nanoscale problems. The conventional continuum assumption breaks down when the system reaches the nanometer scales, sometimes even micrometer scales, and the Navier–Stokes (NS) equations can no longer be used. Molecular dynamics (MD) simulation, as a fully atomistic description, can act as a substitute to describe the fluid flow and heat transfer at such scales. However, MD simulations are highly time-consuming and need lots of computer memory. A multiscale atomistic–continuum method (O'Connell and Thompson 1995; Flekkoy et al. 2000; Delgado-Buscalioni and Coveney 2003; Nie et al. 2004; Tao and He 2009; He and Tao 2012; Zhou et al. 2012) has emerged and becomes popular, which possesses the advantages of both the atomistic and continuum descriptions. In such multiscale methods, MD simulation is used to obtain the microscopic details near the key positions such as interfaces between fluid and solid, where the continuum assumptions break down, and the macro-field of the remaining bulk region can be solved by the continuum mechanics.

The periodic boundary condition (PBC) is often used in MD simulations for homogeneous systems. However, in the multiscale atomistic–continuum methods, PBC is no longer applicable because of inhomogeneity of the atomistic region. In order to remove the periodical condition at the boundary of MD region while still keeping correct mean pressure on the MD system, a boundary force should be applied on atoms near the boundary. Among those existing boundary force models, O'Connell and Thompson (1995) used a constant boundary force $F_b = -\alpha P \rho^{-2/3}$, where α is an adjustable parameter, P the thermodynamic pressure of the system, and ρ the local density. Flekkoy

et al. (2000) proposed another boundary force $F_b = -(g(r_i)/\sum_j g(r_j))PA$, where $g(r)$ is a weight function which diverges to infinity when the distance r between the atom and the boundary approaches zero. Delgado-Buscalioni and Coveney (2003) used the similar boundary force model, except that the weight function $g(r)$ was set to be 1 to ensure the energy conservation. Nie et al. (2004) employed another diverging boundary force $F_b = -\beta P\sigma(r_c - r)/(1 - (r_c - r)/r_c)$, where β acts as an adjustable parameter, and r_c is the cutoff radius. Taking account of the local structure of the fluid, Werder et al. (2005) derived a model by integrating the force exerted by the particles that are located outside of the atomistic region. In their model, the pair potential and the radial distribution function (RDF) were used to implement the integration. It was found that their model could significantly reduce the density perturbations near the boundary compared with other forms of boundary force (O'Connell and Thompson 1995; Flekkoy et al. 2000; Delgado-Buscalioni and Coveney 2003; Nie et al. 2004). However, Kotsalis et al. (2007) pointed out that the model of Werder et al. (2005) was not stable when the fluid state is changed to the liquid regime from supercritical state. They developed an advanced model, in which a dynamic controller based on the information of local density was used to update the boundary force. It was found that this model can keep the density fluctuation at a low level. Recently, Huang et al. (2010) employed a soft constraint mechanism to correct the instantaneous deviation of the local fluid state. The mechanism was found to be stable even under internal disturbance.

In the model developed by Werder et al. (2005), the RDF is crucial to the accuracy of the boundary force. The expressions of RDF introduced by Matteoli and Ali Mansoori (1995) or Bamdad et al. (2006) can be used to perform the integration to obtain the boundary force. However, due to the complexity of the curve shape of the RDF, there are often lots of adjustable parameters in the existing expressions. It is quite difficult to perform the integration with so many adjustable parameters which are dependent on the fluid state. Meanwhile, the deviation of the RDF in Matteoli and Ali Mansoori (1995) from the one obtained from the MD simulation at the same state point could cause the inaccuracy of boundary force (Werder et al. 2005). In addition, the simulations in Werder et al. (2005) and Kotsalis et al. (2007) are both performed at fixed state points, i.e., the density and temperature are known a priori and will not change during the simulations. Thus, their models are not able to deal with the cases in which the density or temperature is not known a priori but needs to be obtained during the simulation, such as the Poiseuille flow with heat transfer. The major purpose of the present paper is to investigate the relationship between the boundary force and the fluid state used in the multiscale atomistic–continuum simulation. The outline of the paper is as follows: In Sect. 2, in order to study the relationship between the boundary force and the fluid state, the equilibrium MD simulations are performed in various state points with periodic boundary condition in all three directions. A fitting formula of the boundary force is proposed based on the relationship, and the accuracy of the formula is verified through additional MD simulations. In Sect. 3, the proposed expression of boundary force is validated through the multiscale atomistic–continuum simulation of Poiseuille flow in which the heat is generated by viscous dissipation of fluid and transferred to the solid wall. In Sect. 4, the unsteady heat transfer problem is simulated to further demonstrate the feasibility of the boundary force model. Finally, some concluding remarks are given in Sect. 5.

2 An expression of boundary force

In this section, the equilibrium MD simulations (Allen and Tildesley 1987; Rapaport 2004) are performed for fluid argon to investigate the relationship between the boundary force and the fluid state including the reduced density and temperature. The following shifted Lennard-Jones (L-J) potential is used to describe the atomic interactions

$$\phi(r) = 4\varepsilon\left[\left(\frac{\sigma}{r}\right)^{12} - \left(\frac{\sigma}{r}\right)^{6} - \left(\frac{\sigma}{r_c}\right)^{12} + \left(\frac{\sigma}{r_c}\right)^{6}\right] \quad (1)$$

where $\varepsilon = 1.67 \times 10^{-21}$ J and $\sigma = 0.341$ nm are the energy and length characteristic parameters for argon, respectively. r_c is a cutoff length beyond which the atomic interactions are not considered. In our simulations, r_c is chosen to be 2.5σ. The equation of motion used to calculate the acceleration of each molecule is

$$m_i \frac{\mathrm{d}^2 \boldsymbol{r}_i}{\mathrm{d}t^2} = -\sum_{j \neq i} \frac{\partial \phi_{ji}}{\partial \boldsymbol{r}_i}. \quad (2)$$

The Newton's equations of motion are then integrated using the leap-frog algorithm with a time step δt of 0.005τ ($\tau = m^{1/2}\sigma\varepsilon^{-1/2}$, m is the mass of argon atom). The MD simulations are performed at a series of different fluid state points in the range of $0.4m\sigma^{-3} \leq \rho \leq 0.9m\sigma^{-3}$ and $1.3\varepsilon/k_B \leq T \leq 3.9\varepsilon/k_B$, and the intervals for densities and temperatures are $0.1m\sigma^{-3}$ and $0.2\varepsilon/k_B$, respectively. Therefore, there are totally $6 \times 14 = 84$ state points to be studied. Periodic boundary conditions are imposed in all three directions. During the simulations, we collect the forces applied on an atom i by all atoms j whose distance from i satisfies $r_{ij} \geq r_w$ and $r_{ij} \leq r_c$, as depicted in Fig. 1. It

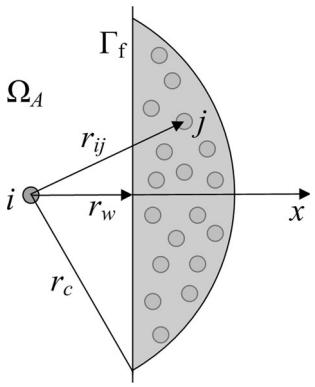

Fig. 1 Schematic for effective boundary force

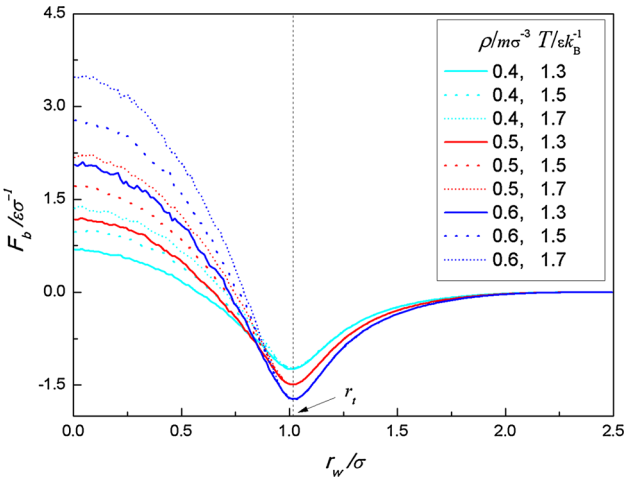

Fig. 2 The boundary force at different fluid states

is worth noting that in Fig. 1, Γ_f is a fictitious boundary that mimics the atomistic boundary in the MD simulations when considering non-periodic boundary condition (NPBC), and r_w is the distance between the atom i and the boundary Γ_f. The position of the boundary Γ_f can be arbitrary in the x direction, because the system is homogenous. Since r_w changes from 0 to r_c, we divide r_c into 200 bins of equal width and obtain the average force in every bin until all have 3×10^6 entries (Werder et al. 2005), i.e., the total number of atoms in any bin during the period of sampling should be larger than 3×10^6.

The change of the boundary force F_b with the distance r_w is shown in Fig. 2. To show it more clearly, data at only nine different fluid state points are given, i.e., for the combination of three different densities and three different temperatures. As can be seen in Fig. 2, at a given fluid state, when r_w becomes larger, F_b decreases from positive to negative until r_w reaches the turning point r_t, which means the atom i feels the repulsive force with small r_w and it feels the attractive force with large r_w. After the turning point r_t, the absolute value of F_b decreases with increase of r_w and gradually approaches 0, which means the attractive force felt by the atom i decreases and then vanishes when the distance r_w approaches r_c. It can also be seen from Fig. 2 that all the curves reach the lowest point at the same turning point r_t for any fluid state studied, at which the attractive force reaches its maximum value. The turning point r_t is found to be $r_t = 1.04\sigma$. In order to make the fitting of boundary force formula easier and more precise, we divide the curves into two parts by the vertical line $r_w = 1.04\sigma$. At the left side, the curves become steeper when the density or the temperature is higher. Moreover, it is observed that the intercept of the curve with the ordinate increases in proportion with the temperature at a fixed density. However, at the right side, the effective force changes only with the density but not with the temperature. The independency on temperature of the right side may be a special characteristic for L-J potential.

Based on the data at 84 different state points, a formula of boundary force can be fitted as

$$F_b = \begin{cases} p_1 + p_2 e^{(r_w+0.25)^{3.4}} \cos(p_3 r_w) & \text{for} \quad r_w \le 1.04\sigma \\ \frac{-1}{q_1 + q_2(2.5-r_w)^2 + \frac{q_3}{(2.5-r_w)^2}} & \text{for} \quad r_w > 1.04\sigma, \end{cases} \tag{3}$$

where p_1, p_2, p_3, q_1, q_2, and q_3 are six parameters, the first three of which are functions of density and temperature and the next three of which are functions of density only. The expressions of the parameters are given as

$$\begin{aligned} p_1 = {} & (-18.953 + 53.369T - 1.253T^2 + 4.599T^3 \\ & + 59.871\ln(\rho) + 19.737(\ln(\rho))^2)/ \\ & (1 + 2.592T - 0.557T^2 + 0.049T^3 \\ & - 13.912\ln(\rho) + 18.657(\ln(\rho))^2) \end{aligned} \tag{4}$$

$$\begin{aligned} p_2 = {} & (-0.094 + 2.808T - 0.019T^2 - 0.001T^3 \\ & + 2.823\ln(\rho) + 2.071(\ln(\rho))^2)/(1 + 0.168T - 0.013T^2 \\ & - 4.323\ln(\rho) + 2.557(\ln(\rho))^2 - 2.155(\ln(\rho))^3) \end{aligned} \tag{5}$$

$$\begin{aligned} p_3 = {} & 3.934 + 0.099T^{0.394} - 0.097\rho^{17.437} \\ & + 0.075T^{0.394}\rho^{17.437} \end{aligned} \tag{6}$$

$$\begin{aligned} q_1 = {} & -30.471 + 113.879\rho - 207.205\rho^2 + 184.242\rho^3 \\ & - 62.879\rho^4 \end{aligned} \tag{7}$$

$$q_2 = 6.938 - 25.788\rho + 46.773\rho^2 - 41.768\rho^3 + 14.394\rho^4 \tag{8}$$

$$\begin{aligned} q_3 = {} & 39.634 - 147.821\rho + 269.519\rho^2 - 239.066\rho^3 \\ & + 81.439\rho^4. \end{aligned} \tag{9}$$

It is worth noting that the involvement of temperature as a variable of the fitting formula is of great significance. It is

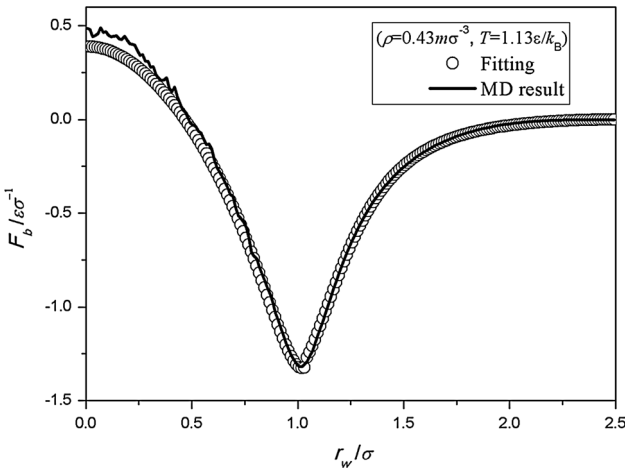

Fig. 3 The boundary force from fitting formulas and MD simulation at $\rho = 0.43m\sigma^{-3}$ and $T = 1.13\varepsilon/k_{\mathrm{B}}$

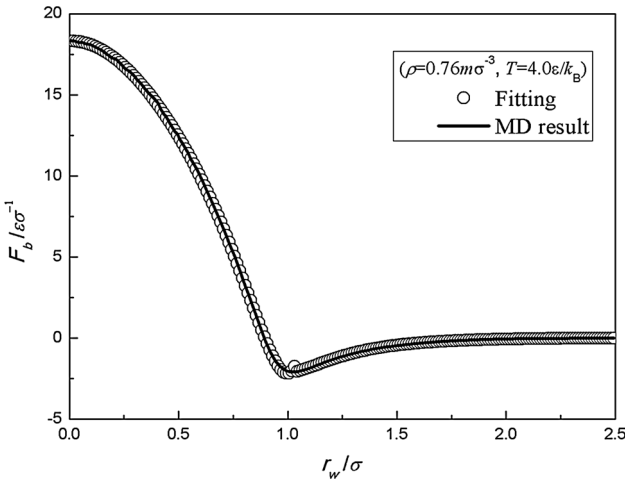

Fig. 4 The boundary force from fitting formulas and MD simulation at $\rho = 0.76m\sigma^{-3}$ and $T = 4.0\varepsilon/k_{\mathrm{B}}$

this involvement that makes our formula be able to be used to the cases with temperature variation.

In order to verify the accuracy of the fitting formula, two additional equilibrium MD simulations at different fluid states ($\rho = 0.43m\sigma^{-3}$, $T = 1.13\varepsilon/k_B$ and $\rho = 0.76\ m\sigma^{-3}$, $T = 4.0\varepsilon/k_B$) are performed. Then, the boundary forces from Eq. (3) are compared with those from MD simulations. It can be seen from Figs. 3, 4 that the boundary forces F_{b} calculated from Eq. (3) agree quite well with MD simulations, except for the minor mismatch at the far-left part of the curve. During the simulation, we found that as the density of fluid decreases, the fluctuation of the equilibrium MD simulation results becomes more severe, which can be seen from the left part of curve in Fig. 3. Therefore, the minor mismatch at the far-left part of the curve in Fig. 3 is reasonable (Fig. 4).

3 Poiseuille flow

In this section, the fitting formula given in Eq. (3) is used as the boundary force of the multiscale atomistic–continuum simulation. As shown in Fig. 5a, in the multiscale simulation, the domain decomposition method is used and the computational domain is divided into three regions: a continuum region named C region where the flow can still be described by NS equations and the finite volume method is used as a solver, an atomistic region named P region where the MD method is employed and an overlap region named O region where a coupling scheme is applied to ensure the continuity of the state variables, including velocity and temperature in the present paper.

MD simulation introduced above is carried out in P region. The fluid density is set to be $\rho = 0.81m\sigma^{-3}$, and the cutoff length $r_c = 2.5\sigma$. In order to control the temperature of the solid wall, the "phantom method" (Maruyama and Kimura 1999; Yi et al. 2002) is used. As can be seen in Fig. 5b, the solid wall at the bottom of P region consists of three layers of fcc (1 1 1) surface of "real" atoms. The distance of nearest neighbor atoms $\sigma_w = 0.814\sigma$ and the spring constant $k = 3249.1\varepsilon\sigma^{-2}$. Right below the "real" atoms, there are another two layers of "phantom" atoms. Taking account of the interaction between the "real" and "phantom" atoms, a special spring of $2\,k$ in vertical direction and $0.5\,k$ in horizontal direction is set between the third "real" layer and the upper "phantom" layer, and another spring of $2\,k$ in vertical direction and $3.5\,k$ in horizontal direction is set between two "phantom" layers. The temperature of the upper "phantom" layer is controlled to be $T_w = 1.1\varepsilon/k_{\mathrm{B}}$ by Langevin method (Maruyama and Kimura 1999; Tully 1980). The interaction between fluid and solid is also calculated by Eq. (1), except that the characteristic parameters are changed to $\sigma_{\mathrm{ls}} = 0.91\sigma$ and $\varepsilon_{\mathrm{ls}} = \varepsilon$ which yields a slip boundary condition at the solid wall (Sun et al. 2010; Li and Xu 2006; Xu and Li 2007).

For C region, the two-dimensional incompressible NS equations are solved (Tao 2001)

$$\nabla \cdot u = 0 \tag{10}$$

$$\frac{\partial u}{\partial t} + u \cdot \nabla u = \frac{\mu}{\rho}\nabla^2 u - \frac{1}{\rho}\nabla p \tag{11}$$

$$\frac{\partial T}{\partial t} + u \cdot \nabla T = \frac{\lambda}{\rho c}\nabla^2 T + \frac{2\mu}{\rho c}\left[\left(\frac{\partial u}{\partial x}\right)^2 + \left(\frac{\partial w}{\partial z}\right)^2 + \frac{1}{2}\left(\frac{\partial u}{\partial z} + \frac{\partial w}{\partial x}\right)^2\right] \tag{12}$$

where u and w are the velocity components in the x and z directions; μ, c, and λ are the dynamic viscosity, specific

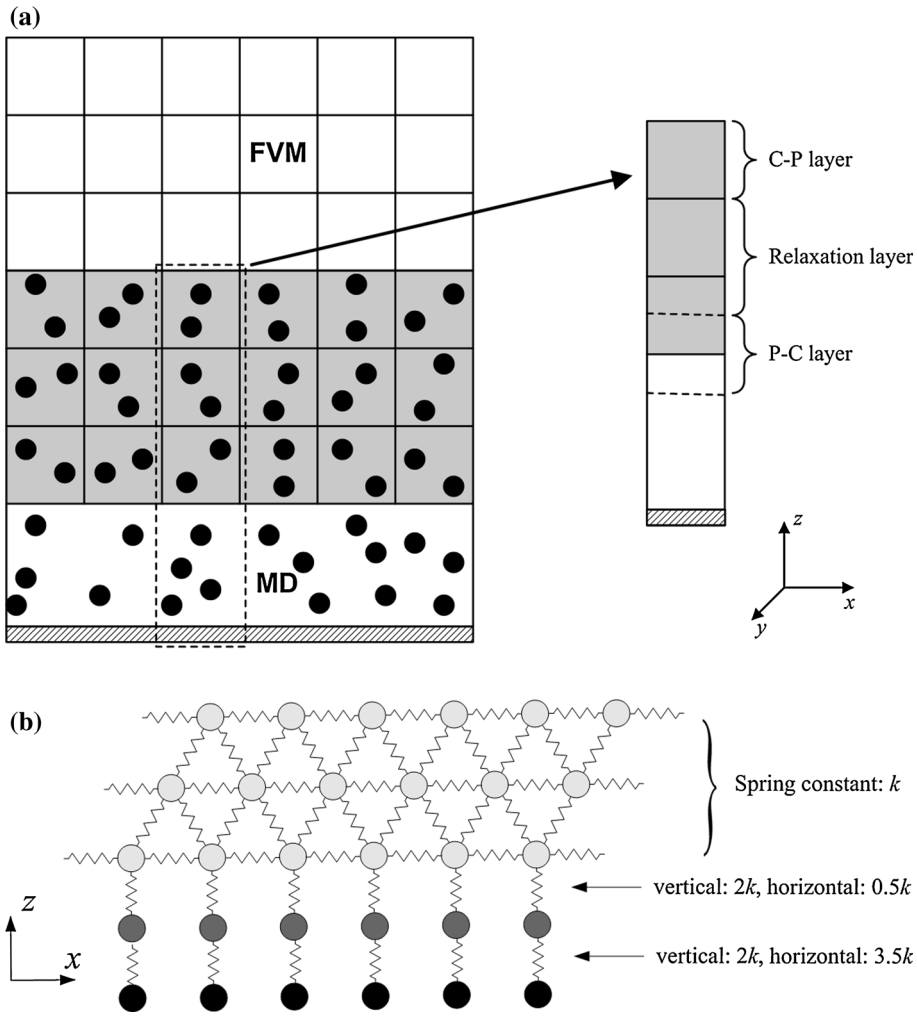

Fig. 5 Schematic of the multiscale simulation. **a** Domain decomposition; **b** Atom arrangement of solid wall

heat, and thermal conductivity, respectively. These thermophysical properties are obtained from the property database of fluid (NIST 2005) such as $\mu = 2.18\varepsilon\tau\sigma^{-3}$, $c = 2.40k_{\mathrm{B}}m^{-1}$, and $\lambda = 6.92k_{\mathrm{B}}\sigma^{-1}\tau^{-1}$, which corresponds to the mean fluid state of $\rho = 0.81m\sigma^{-3}$and $T = 1.25\varepsilon/k_{\mathrm{B}}$ of argon. The semi-implicit method for pressure-linked equations consistent algorithm is used to solve the NS equations (Tao 2001). In order to validate the fitting formula of the boundary force proposed in the last section, we simulate the Poiseuille flow with viscous dissipation by multiscale simulation. As shown in Fig. 6, only a half-channel l_z ($l_z = H/2$, $H = 41.74\sigma$ is the height of the channel) needs to be simulated because of symmetry. For the simulation domain, the size of P region is set as $l_x^{\mathrm{P}} = 8.70\sigma$, $l_y^{\mathrm{P}} = 4.64\sigma$ and $l_z^{\mathrm{P}} = 13.92\sigma$, and the size of C region is $l_x^{\mathrm{C}} = l_z^{\mathrm{C}} = 13.92\sigma$. C region is divided by uniform grids with the grid size $\Delta x^{\mathrm{C}} = \Delta z^{\mathrm{C}} = 2.32\sigma$. The boundary conditions are as follows: the top boundary of C region is set to be symmetric, and the maximum velocity at this boundary is fixed as $U_{\mathrm{m}} = 1.196\sigma\tau^{-1}$; the inlet and outlet boundaries along the flow direction are periodic boundary conditions; the bottom boundary of C region is updated with the information from P region and the state variables such as u, w, and T are assumed to be constant along the flow direction.

The overlap region is divided into three layers: C–P layer, relaxation layer, and P–C layer (see Fig. 5). The data transfer from P region to C region in P–C layer is relatively simple since it is easy to extract the macroscopic quantities from a large amount of data at nanoscale level by averaging. However, it is difficult to implement the reverse procedure. In C–P layer, the acceleration of the ith atom should be adjusted as follows (Nie et al. 2004):

$$\ddot{\mathbf{r}}_i(t) = \frac{1}{\delta t^{\boldsymbol{P}}}\left[\mathbf{u}(t+\delta t^{\boldsymbol{P}}) - \frac{1}{N^{\boldsymbol{C-P}}}\sum_{j=1}^{N^{C-P}}\dot{\mathbf{r}}_j(t)\right] + \left[\frac{\mathbf{f_i(t)}}{m} - \frac{1}{N^{\boldsymbol{C-P}}}\sum_{j=1}^{N^{C-P}}\frac{\mathbf{f_j(t)}}{m}\right] \tag{13}$$

where $\mathbf{u}(t + \delta t^{\mathrm{P}})$ is the velocity vector of the center of C–P layer at the moment $t + \delta t^{\mathrm{P}}$ and it is obtained from the continuum solutions of C region, $N^{\mathrm{C-P}}$ is the number of

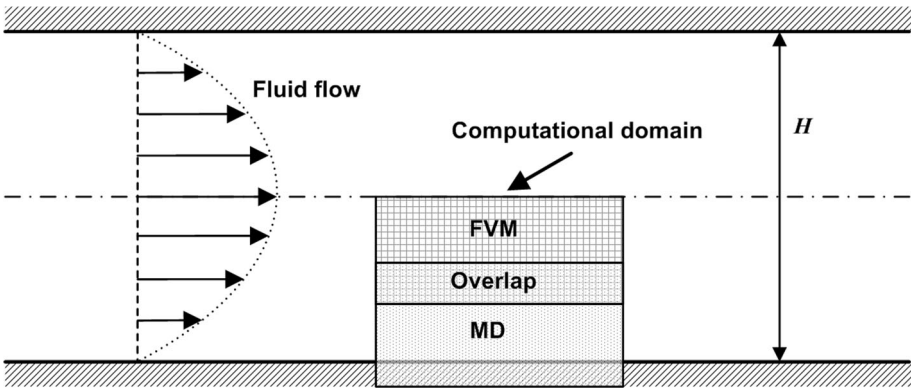

Fig. 6 Schematic of the multiscale simulation for Poiseuille flow with viscous dissipation

atoms in C–P layer, $\mathbf{f}_i$ and $\mathbf{f}_j$ are the forces on ith and jth atoms in C–P layer caused by interactions with other atoms. In addition, an external driving force needs to be applied to all the atoms in P region to take the pressure gradient $-\mathrm{d}p/\mathrm{d}x$ into account:

$$f_p = -\frac{m}{\rho}\left(\frac{\mathrm{d}p}{\mathrm{d}x}\right). \tag{14}$$

In a half-channel Poiseuille flow problem, we need two conditions to make the solution determined, usually they are boundary velocity at the wall (U_s) and symmetry at the central line, if the pressure gradient $\mathrm{d}p/\mathrm{d}x$ is already known. However, for the present problem, we cannot predetermine either U_s or $\mathrm{d}p/\mathrm{d}x$ due to the slippage of the wall, so we need an extra condition, i.e., maximum velocity at central line (U_m). On the other hand, $\mathrm{d}p/\mathrm{d}x$ and U_m are actually equivalent conditions (either can be calculated directly from the other in non-slip flows), so we fix the maximum velocity at central line U_m in the present study. Note that if we calculate $\mathrm{d}p/\mathrm{d}x$ based on the convergent solution and rerun it with the conditions of symmetry at the central line and fixed $\mathrm{d}p/\mathrm{d}x$, we can achieve identical solutions.

The coupling of temperature is achieved by using Langevin method (Tully 1980) only in y direction in C–P layer. More details about the coupling scheme of velocity and temperature can be found in (Sun et al. 2010).

In order to apply the proper mean pressure on the boundary of P region, the boundary force model proposed in Sect. 2 is employed. Here, the fitting formula in Eq. (3) is only used to atoms whose distance from the top boundary of P region is less than the cutoff radius r_c. The reason why Poiseuille flow with viscous dissipation is chosen to demonstrate our fitting formula is that during the simulation, the temperature at the boundary of P region is changing because of viscous dissipation and cannot be known a priori. In our simulation, the temperature T in Eq. (3) is updated by the continuum solutions at the boundary of P region. To avoid the atoms drifting away from P region, the specular wall model developed in (Werder et al. 2005) is adopted. Meanwhile, the boundary force model from (Nie et al. 2004) is also applied as a reference, which says:

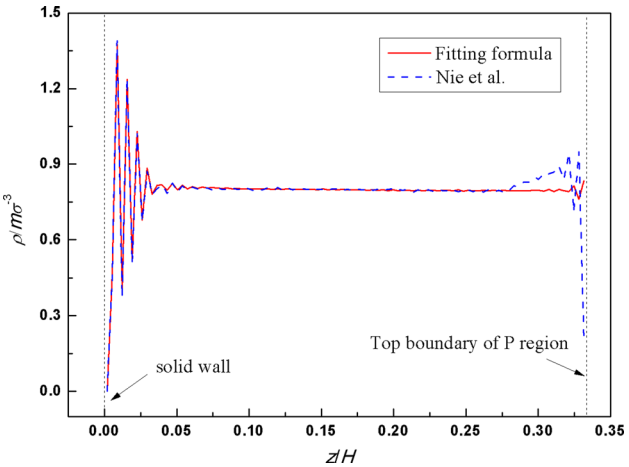

Fig. 7 Comparison of density profiles from our fitting formula and Nie et al.'s model

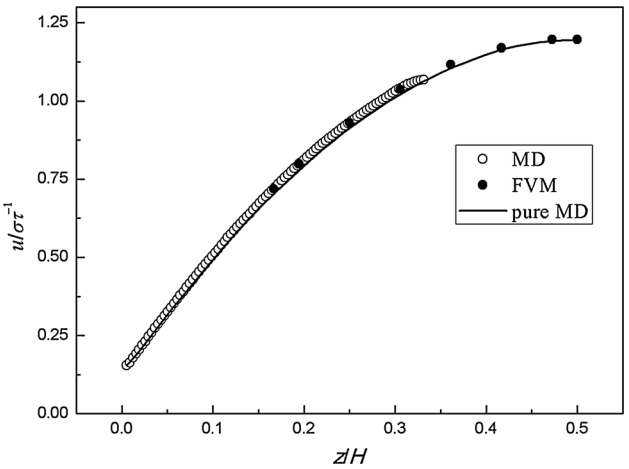

Fig. 8 Comparison of velocity profiles from multiscale simulation and pure MD result

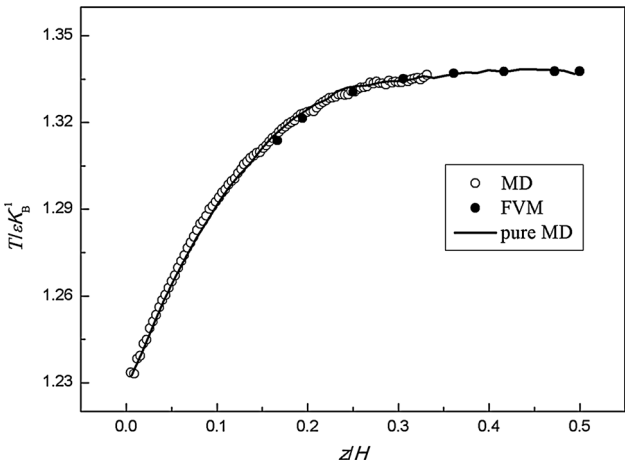

Fig. 9 Comparison of temperature profiles from multiscale simulation and pure MD result

$$F_b = -\beta P\sigma(r_c - r_w)/(1 - (r_c - r_w)/r_c). \quad (15)$$

Figure 7 shows the density profiles along the z direction in P region. It can be seen that the oscillatory characteristics of density profiles near the solid wall by the model of Nie et al. (2004) and our fitting formula Eq. (3) are almost the same. This phenomenon reflects the fact that the liquid atoms distribute orderly near the solid wall due to strong solid–liquid interactions. However, there is strong oscillation adjacent to the top boundary of P region by the model of Nie et al. (2004), and it extends a relatively long distance into P region. The oscillation is effectively eliminated when using our fitting formula. In Yen et al.'s work (2007), a depress region located above C–P region was employed to apply the external force to prevent atoms from drifting away. They used Nie et al.'s force model (2004) in depress region and found the similar density oscillation phenomenon. The unrealistic density oscillation may result in unnecessary disturbances to the atomistic region (Kotsalis et al. 2007). Consequently, they ignored the MD results in depress region and replaced it by continuum solution. The depress region is not needed when using our fitting formula of the boundary force; hence, the size of P region is reduced and the efficiency of multiscale simulation is improved. Figures 8 and 9 show the profiles of velocity and temperature, respectively. It can be seen that the results of multiscale simulation agree quite well with the pure MD predictions, with the maximum relative deviations of 2.7 and 2.2 % for velocity and temperature, respectively. This confirms the correctness of our fitting formula of boundary force. It is worth noting that as far as the computational times are concerned, the computational time of multiscale simulation for this problem is only one-third of the pure MD, once again showing the advantage of the multiscale simulation approach.

4 Unsteady heat transfer

To further test our fitting formula, we studied the unsteady heat transfer problem between two stationary solid walls. The temperature of the entire system including two walls and the liquid argon was kept at $1.1\varepsilon/k_B$ for 100τ at the beginning of simulation. After the period of equilibrium, the temperature of the top wall was suddenly changed to $1.3\varepsilon/k_B$ at $t = 0$, while the temperature of the bottom wall was still kept at $1.1\varepsilon/k_B$. The thermostat for the liquid argon was then switched off. For the heat transfer problem, the solid walls are constructed with Fe atoms. The more realistic embedded atom model (EAM) is used and the relevant parameters for the EAM model are proposed by Mendelev et al. (2003). The Fe–Ar interaction is also modeled with L–J potential, and the characteristic parameters are $\sigma_{ls} = 1.09\sigma$ and $\varepsilon_{ls} = 5\varepsilon$ (Balasubramanian et al. 2008). For each solid wall, there are three layers of Fe atoms of which the outermost one is fixed, and the temperature of wall is adjusted by rescaling the velocities of atoms in the two remaining layers (Balasubramanian et al. 2008). The channel height is 235σ in z direction. Different from the Poiseuille flow problem, the whole domain should be simulated for the hybrid simulation here, i.e., there are two MD subdomains which are near the bottom ($0 \le z \le 76.4\sigma$) and top wall ($158.6\sigma \le z \le 235\sigma$), respectively, and a continuum region in between ($58.7\sigma \le z \le 176.2\sigma$). For the temperature coupling in C–P layer, all thermostat methods introduce an additional time lag (Liu et al. 2007). Although Langevin thermostat is appropriate for steady-state problems, it introduces more severe time lag than velocity rescaling method used in Allen and Tildesley (1987) and Liu et al. Liu et al. (2007) for unsteady heat transfer problems. Therefore, the velocity rescaling method (Allen and Tildesley 1987; Liu et al. 2007) is adopted here, which is given as follows:

$$\mathbf{u} = \bar{\mathbf{u}} + (T_{target}/T_{MD})^{1/2}(\mathbf{u} - \bar{\mathbf{u}}) \quad (16)$$

where $\bar{\mathbf{u}}$ is the mean velocity of C–P layer, T_{target} is the target temperature from the continuum region, and T_{MD} is the microscopic temperature of C–P layer.

All of our MD simulations in this section are carried out by the large-scale atomic/molecular massively parallel simulator (Plimpton 1995) while self-programming codes are used for simulations in above sections.

Figure 10 shows the comparison of the evolutions of the temperature profiles obtained from multiscale and pure MD simulations. The multiscale results agree well with pure MD results, except that there exists an obvious deviation for the time interval from $t = 0$ to $1{,}500\tau$, which cannot be reduced by averaging over more independent simulations. The similar phenomenon was also found in Liu et al. (2007).

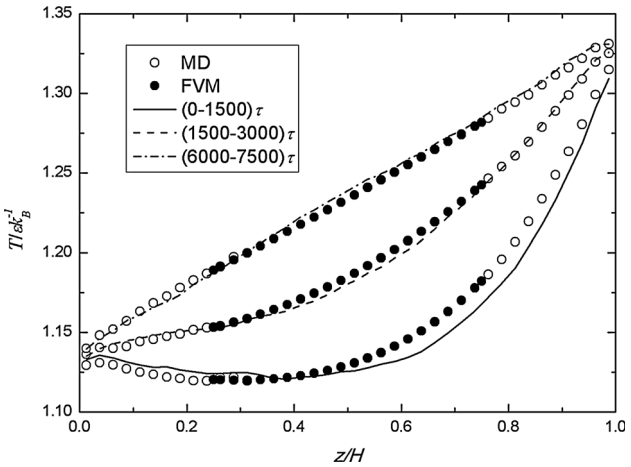

Fig. 10 Comparison of temperature profiles at different times for unsteady heat transfer from multiscale simulation and pure MD result

5 Conclusions

In the present work, the implementation of NPBC which is often used in the multiscale atomistic–continuum simulations has been investigated. Based on the relationship between the boundary force and the fluid state at the boundary, a fitting formula of the boundary force is proposed. The accuracy of the fitting formula is verified through the equilibrium MD simulations. The proposed fitting formula for the boundary force has also been employed in a multiscale Poiseuille simulation with viscous dissipation. The elimination of density oscillation near the boundary of atomistic region demonstrates the correctness of the fitting formula, which has been further proven by the good agreement of velocity and temperature profiles between the multiscale simulation and the pure MD results. Finally, the proposed fitting formula has been adopted to simulate an unsteady heat transfer problem between two stationary solid walls. The good agreement in evolutions of temperature with time from pure MD and multiscale simulation further confirms the feasibility of the proposed boundary force formula.

Furthermore, the application of our fitting formula is quite convenient since the fluid state including density and temperature near the boundary does not need to be known a priori. The boundary force can easily be given by our fitting formula based on the boundary information during the computational procedure. Also, we believe that our fitting formula can be used for other complicated MD boundaries, such as the arbitrary boundaries studied in Borg et al. (2010).

However, there are some limits of our boundary force model: Firstly, it can only be used for L–J potential since the fitting formula is constructed based on the L–J potential, a more universal model needs to be developed in the future. Secondly, it cannot be used for gas. Thirdly, it cannot be used for polyatomic molecules such as water.

Acknowledgments This work is supported by the Key Projects of National Natural Science Foundation of China (No. 51136004) and the 12th 5-year National Key Technology R&D Program (2012BAJ02B03). The authors thank the Shanghai Supercomputer Center for computing time.

References

Allen MP, Tildesley DJ (1987) Computer simulation of liquids. Clarendon Press, Oxford

Balasubramanian G, Banerjee S, Puri IK (2008) Unsteady nanoscale thermal transport across a solid-fluid interface. J Appl Phys 104:064306

Bamdad M, Alavi S, Najafi B, Keshavarzi E (2006) A new expression for radial distribution function and infinite shear modulus of Lennard-Jones fluids. Chem Phys 325:554–562

Borg MK, Macpherson GB, Reese JM (2010) Controllers for imposing continuum-to-molecular boundary conditions in arbitrary fluid flow geometries. Mol Simulat 36:745–757

Delgado-Buscalioni R, Coveney PV (2003) Continuum-particle hybrid coupling for mass, momentum, and energy transfers in unsteady fluid flow. Phys Rev E 67:046704

Flekkoy EG, Wagner G, Feder J (2000) Hybrid model for combined particle and continuum dynamics. Europhys Lett 52:271–276

He YL, Tao WQ (2012) Multiscale simulations of heat transfer and fluid flow problems. J Heat Transf T ASME 134:031018

Huang ZG, Guo ZN, Yue TM, Chan KC (2010) Non-periodic boundary model with soft transition in molecular dynamics simulation. Europhys Lett 92:50007

Kotsalis EM, Walther JH, Koumoutsakos P (2007) Control of density fluctuations in atomistic–continuum simulations of dense liquids. Phys Rev E 76:016709

Li YX, Xu JL (2006) A new criterion number for the boundary conditions at the solid/liquid interface in nanoscale. Nanosc Microsc Therm 10:109–141

Liu J, Chen SY, Nie XB, Robbins MO (2007) A continuum-atomistic simulation of heat transfer in micro- and nano-flows. J Comput Phys 227:279–291

Maruyama S, Kimura T (1999) A study on thermal resistance over a solid-liquid interface by the molecular dynamics method. Therm Sci Eng 7:63–68

Matteoli E, Ali Mansoori G (1995) A simple expression for radial distribution functions of pure fluids and mixtures. J Chem Phys 103:4672–4677

Mendelev MI, Han S, Srolovitz DJ, Ackland GJ, Sun DY, Asta M (2003) Development of new interatomic potentials appropriate for crystalline and liquid iron. Philos Mag 83:3977–3994

National Institute of Standards and Technology (NIST) (2005) Thermophysical properties of fluid systems. http://webbook.nist.gov/chemistry/fluid/

Nie XB, Chen SY, E WN, Robbins MO (2004) A continuum and molecular dynamics hybrid method for micro- and nano-fluid flow. J Fluid Mech 500:55–64

O'Connell ST, Thompson PA (1995) Molecular dynamics-continuum hybrid computations: a tool for studying complex fluid flows. Phys Rev E 52:R5792

Plimpton SJ (1995) Fast parallel algorithms for short-range molecular dynamics. J Comput Phys 117:1–19

Rapaport DC (2004) The art of molecular dynamics simulation, 2nd edn. Cambridge University Press, Cambridge

Sun J, He YL, Tao WQ (2010) Scale effect on flow and thermal boundaries in micro-/nano-channel flow using molecular dynamics–continuum hybrid simulation method. Int J Numer Meth Eng 81:207–228

Tao WQ (2001) Numerical heat transfer (2nd edn). Xi'an Jiaotong University Press, Xi'an

Tao WQ, He YL (2009) Recent advances in multiscale simulation of heat transfer and fluid flow problems. Prog Comput Fluid Dy 9:150–157

Tully JC (1980) Dynamics of gas-surface interactions: 3D generalized langevin model applied to fcc and bcc surfaces. J Chem Phys 73:1975–1985

Werder T, Walther JH, Koumoutsakos P (2005) Hybrid atomistic–continuum method for the simulation of dense fluid flows. J Comput Phys 205:373–390

Xu JL, Li YX (2007) Boundary conditions at the solid-liquid surface over the multiscale channel size from nanometer to micro. Int J Heat Mass Transf 50:2571–2581

Yen T, Soong C, Tzeng P (2007) Hybrid molecular dynamics-continuum simulation for nano/mesoscale channel flows. Microfluid Nanofluid 3:665–675

Yi P, Poulikakos D, Walther J, Yadigaroglu G (2002) Molecular dynamics simulation of vaporization of an ultra-thin liquid argon layer on a surface. Int J Heat Mass Transf 45:2087–2100

Zhou WJ, Luan HB, Sun J, He YL, Tao WQ (2012) A molecular dynamics and lattice boltzmann multiscale simulation for dense fluid flows. Numer Heat Transf B Fund 61:369–386